A Comparative Study of Mixed Phosphate-Pyrophosphate Materials for Aqueous and Non-Aqueous Na-ion Batteries

Gintarė Gečė,[a,b] Maider Zarrabeitia,[b,c] Jurgis Pilipavičius,[a,d] Stefano Passerini,[b,c,e] Linas Vilčiauskas*[a]

[a] Center for Physical Sciences and Technology (FTMC), Saulėtekio al. 3, LT-10257 Vilnius, Lithuania
[b] Helmholtz Institute Ulm (HIU), Helmholtzstrassse 11, 89081 Ulm, Germany
[c] Karlsruhe Institute of Technology (KIT), P.O. Box 3640, 76021 Karlsruhe, Germany
[d] Insitute of Chemistry, Vilnius University, Saulėtekio al. 3, LT-10257 Vilnius, Lithuania
[e] Chemistry Department, Sapienza University, Piazzale A. Moro 5, 00185 Rome, Italy
* linas.vilciauskas@ftmc.lt

Abstract

Na-ion batteries based on abundant and sustainable materials might become one of the leading alternative technologies especially suitable for large-scale stationary storage. Various (mixed)phosphate framework materials are attracting much interest mainly due to their high structural stability and diversity. In this study, we report on the successful synthesis of mixed phosphate-pyrophosphate $Na_7V_4(PO_4)(P_2O_7)_4$, $Na_4Fe_3(PO_4)_2P_2O_7$, and $Na_4Mn_3(PO_4)_2P_2O_7$. The electrochemical properties of these materials are comprehensively characterized in different organic and aqueous electrolytes. The findings reveal that $Na_7V_4(PO_4)(P_2O_7)_4$ and $Na_4Fe_3(PO_4)_2P_2O_7$ exhibit very good cycling performance and rate capability in organic solvent-based electrolytes. However, their performance deteriorates significantly even in 'water-in-salt' aqueous electrolytes due to the rapid electrochemical degradation. $Na_4Mn_3(PO_4)_2P_2O_7$ demonstrates limited electrochemical activity in organic electrolytes and virtually no activity in 'water-in-salt' electrolytes, likely due to degradation processes resulting in blocking interphasial layers on electrode particles. These results underscore the need for further research to optimize the performance of these materials and identify potential strategies for enhancing their stability and activity in different electrolytes.

INTRODUCTION

Rechargeable Na-ion batteries are deemed to become a preferred technology for large-scale electrochemical energy storage systems.[1] To compete with more mature Li-ion batteries, they must significantly outscore them on several metrics, the most important being materials availability and sustainability.[2,3] In terms of Na-based electrode materials, three distinct classes are currently the most studied. They are transition metal layered oxides, hexacyanometallates, and polyanion compounds.[4] Phosphate framework materials are highly interesting due to their stability, safety, low cost, and structural diversity.[5] The latter is due to the ability to host many different cations and swap anions in their structure. Many

subclasses can be formed by combining different anions such as PO_4^{3-}, $P_2O_7^{4-}$, CO_3^{2-}, SO_4^{2-}, F^- etc.[6] The combination of different anions not only affects the structural but also the electrochemical properties of these materials.[7] For example, changing some of PO_4^{3-} by $P_2O_7^{4-}$, typically results in lower thermal stability but pyrophosphate units show stronger inductive effect resulting in higher redox potential and energy density.[8] Although the introduction of anions like SO_4^{2-} might have an even stronger inductive effect, they are also typically not stable above 400 °C and might be soluble in aqueous electrolytes limiting the practical applicability of such materials in diverse electrolytes.[9]

Current research on novel polyanionic phosphate electrode materials mostly focuses on V-, Fe- and Mn-based compounds. This is mainly due to the high electrode potential of these metals, and/or their relative abundance and low-cost.[10] According to several reports, $Na_4X_3(PO_4)_2P_2O_7$ ($X^{(II)}$ = Fe, Mn, Co, Ni,) are very attractive positive electrodes for Na-ion batteries.[7,11–13] They typically crystalize in $Pn2_1a$ (No. 33) space group, and the crystal framework contains infinite $[X_3P_2O_{13}]_\infty$ layers parallel to *b,c* plane, which comprise three $[XO_6]$ octahedra, two $[PO_4]$ tetrahedra, and $[P_2O_7]$ groups along *a*-axis. The neighboring $[X_3P_2O_{13}]_\infty$ structure is interconnected via $[P_2O_7]$ groups along the *a*-axis. These links open facile Na^+ transport pathways along the *b*-axis. Such open 3D Na^+ diffusion channels give rise to fast kinetics and high-rate performance.[14,15]

$Na_4Fe_3(PO_4)_2P_2O_7$, with a relatively high theoretical capacity of 129.0 mAh g^{-1} and an average potential of ~3.1 V vs Na^+/Na, could be synthesized by the conventional solid-state route and showed decent electrochemical performance, rate capability, and charge capacities in both organic and aqueous electrolytes.[16–20] $Na_4Mn_3(PO_4)_2P_2O_7$, with its similar theoretical capacity of 129.6 mAh g^{-1} and expected potential of ~3.8 V vs Na^+/Na showed poor cycling stability, low capacity and rate capability in almost all previous reports,[21–26] except for the work of Kim *et al*. where a reversible capacity of ~121 mAh g^{-1} was delivered at C/20 rate.[21] In the family of mixed-polyanion compounds, $Na_7V_4(PO_4)(P_2O_7)_4$, which has a different space group ($P\underline{4}2_1c$, No. 114) but a similar 3D framework, stands out with its high electrode redox potential of ~4.0 V vs Na^+/Na but slightly lower theoretical capacity of 92.8 mAh g^{-1}. Several reports have shown impressive cycling stability and capacity retention of >78% after 1000 cycles for this material in organic electrolytes.[27,28]

Herein, we report a successful synthesis of $Na_7V_4(PO_4)(P_2O_7)_4$, $Na_4Fe_3(PO_4)_2P_2O_7$ and $Na_4Mn_3(PO_4)_2P_2O_7$ mixed polyanionic materials. A comprehensive comparative study of these materials to understand the influence of the transition metal in terms of their electrochemical performance and stability as Na-ion battery electrodes in a series of aqueous and non-aqueous electrolytes is presented.

EXPERIMENTAL

Materials Preparation

$Na_7V_4(PO_4)(P_2O_7)_4$ (NVPP), $Na_4Fe_3(PO_4)_2P_2O_7$ (NFPP) and $Na_4Mn_3(PO_4)_2P_2O_7$ (NMPP) were synthesized by conventional solid-state methods. For the synthesis of NVPP, Na_2CO_3 (0.9632 g, Glentham, 99+%), NH_4VO_3 (1.2149 g, Reachem, 99.5%), and $NH_4H_2PO_4$ (2.6880 g, Honeywell, 99+%) were mixed using wet (2-propanol) ball milling at 350 rpm for 2 h. The dried mixture was calcined at 600 °C for 5 h and subsequently at 800 °C for 10 h, in N_2/H_2 (95/5%)

atmosphere. For the synthesis of NFPP, $Na_4P_2O_7$ (1.7068 g, ChemPur, p.a.), $FeC_2O_4{\cdot}2H_2O$ (3.4629 g, Chempur, p.a.), and $NH_4H_2PO_4$ (1.4762 g, Honeywell, 99+%) were mixed using wet (2-propanol) ball milling at 350 rpm for 2 h. The dried mixture was calcined at 300 °C for 6 h and subsequently at 500 °C for 12 h, in N_2 atmosphere. For the synthesis of NMPP, $Na_4P_2O_7$ (2.1561 g, ChemPur, p.a.), MnC_2O_4 (2.0730 g, ChemPur, p.a.), and $NH_4H_2PO_4$ (1.1120 g, Honeywell, 99+%) were mixed using wet (2-propanol) ball milling at 350 rpm for 2 h. The dried mixture was calcined at 300 °C for 6 h and subsequently at 600 °C for 6 h, all in ambient air. All obtained materials were post-processed at 350 rpm for 2 h using high-energy planetary ball milling (Retsch, PM400). Then the particles were carbon coated by homogeneously mixing active material (80 wt%) and citric acid (20 wt%, Glentham, 99.5+%) in deionized water, drying the resulting mixture at 80 °C for water elimination, and pyrolyzing it at 500 °C for 12 h, at 600 °C for 6 h, and at 700 °C for 2 h in flowing N_2 atmosphere for NFPP, NMPP and NVPP, respectively. The obtained black powders were again ball milled at 350 rpm for 2 h in order to achieve a uniform final particle size distribution.

Materials Characterization

Powder X-ray diffraction (XRD) patterns were recorded on Bruker Advance D8 diffractometer with Cu radiation ($K_{\alpha 1,2}$ λ = 1.5406 Å, 1.5444 Å) within the range $10° \leq 2\theta \leq 70°$. The scanning speed and step width were 1 min^{-1} and 0.03°, respectively. Rietveld refinements were performed using GSAS-II software suite [29]. The morphological characterization was carried out using a Hitachi SU-70 scanning electron microscope. Thermogravimetric analysis (TGA) for determining carbon content was carried out on a STA600 Perkin-Elmer analyzer in the range of 30 to 700 °C at a heating rate of 20 °C min^{-1} in air atmosphere (20 ml min^{-1}).

Electrochemical Characterization

The electrode slurry was prepared by mixing 70 wt% of active material, 20 wt% of carbon black (CB) (Super-P, TIMCAL), and 10 wt% of polyvinylidene fluoride (PVDF) (HSV1800, Kynar) in N-methyl-2-pyrrolidone (NMP) (Sigma Aldrich, 99.5%). The slurry was homogenized in a planetary ball-mill for 1 h at 175 rpm and 2 h at 350 rpm and then cast as a film which was subsequently dried in a vacuum oven for 3 h at 120 °C. The resulting electrode film was pressed on 316L stainless steel (SS) mesh (#325) and punched into discs (12 mm in diameter) with an average active material loading of ~0.9 mg cm^{-2} for testing them in aqueous electrolytes. The electrochemical properties of the electrodes were characterized in three-electrode T-type cells with a separate reference electrode. For non-aqueous electrolyte cells, 1M $NaPF_6$ (FluoroChem, battery grade) in either diglyme (Sigma-Aldrich, anhydrous, 99.5%) or ethylene carbonate (EC, UBE, battery grade): diethyl carbonate (DEC, UBE, battery grade) (3:7 by volume) organic solutions were used. T-type cells were assembled in an Ar-filled glovebox (MBraun, H_2O and O_2 < 0.1 ppm) using sodium metal (99.8%, Across Organics) as counter and reference electrodes. For the aqueous electrolyte cells, 1M Na_2SO_4 (Lach-ner, 99.3%), 17m $NaClO_4$ (Alfa-Aesar, 98%), 8m NaTFSI (Solvionic, 99.5%), 28m Kac + 8m NaAc ((Potassium Acetate+Sodium Acetate) VWR, 99.5%) solutions were studied. In this case, T-type cells were assembled in ambient atmosphere using Ag/AgCl/3.4M $KCl_{(aq.)}$ as reference and self-standing carbon pellets as counter electrodes. Cyclic voltammetric (CV) measurements were performed on a potentiostat-galvanostat (SP-240, Biologic). Galvanostatic charge-discharge

(GCD) cycling and rate capability experiments were carried out in battery testers (MACCOR, Series 4000 and Neware CT-4008).

RESULTS AND DISCUSSION

Structural and Morphological Characterization

The successful synthesis of solid-state prepared NVPP, NFPP and NMPP was confirmed by powder X-ray diffractometry (XRD). The NVPP powder XRD pattern and its Rietveld refinement results are presented in Figure 1 (a). The presence of sharp diffraction peaks indicates high sample crystallinity and are consistent with the tetragonal space group $P\underline{4}2_1c$ (No. 114).[30] The lattice parameters were determined to be *a* = 14.22427(13) Å, *c* = 6.37216(9) Å and V = 1289.28(3) Å^3. However, $Na_3V_2(PO_4)_3$ (~10.2 wt%) and $NaVP_2O_7$ (~6.6 wt%) impurities were also detected, which is common in the conventional solid-state synthesis of this material.[27,31] The NFPP XRD pattern and its Rietveld refinement results presented in Figure 1 (b) also display the presence of sharp diffraction peaks, indicating high crystallinity. The observed peaks are consistent with the orthorhombic space group $Pna2_1$ (No. 33),[32] showing a pure phase. The resulting lattice parameters were determined to be *a* = 18.0892(10) Å, *b* = 10.6565(6) Å, *c* = 6.5401(3) Å and V = 1260.72(15) Å^3. The NMPP powder XRD and its Rietveld refined patterns are presented in Figure 1 (c) and also show the presence of sharp diffraction peaks indicative of high crystallinity. It is consistent with the orthorhombic space group $Pna2_1$ (No. 33).[21] The resulting lattice parameters were determined to be *a* = 17.99993(27) Å, *b* = 10.74550(17) Å, *c* = 6.64863(10) Å and V = 1285.97(4) Å^3. However, $NaMnPO_4$ (~22.0 wt%) impurity was detected in the NMPP sample. Overall, the powder XRD analysis results confirm that desired phase of NVPP, NMPP, and NFPP with determined lattice parameters which are in good agreement with the literature data,[30,32,21] were successfully prepared by conventional solid-state synthesis.

The morphology of the samples was characterized by Scanning Electron Microscopy (SEM). In all samples, conventional solid-state synthesis yields particles which are of irregular shape and broad size distribution. The mean feature size is in the order of several micrometers (Figure 2). Only NVPP shows slightly larger particles which seem a little bit more sintered together. This could be attributed to higher synthesis temperature.

As described in Experimental section, all samples were additionally coated by a carbon layer using post-synthetic pyrolysis of citric acid to improve electronic contacts between the ceramic particles. It has been previously shown that such treatment does not alter the main phase structure, morphology, and particle size distribution of materials.[36] The resulting carbon content obtained by this procedure was evaluated by TGA and found to be 2.97 wt%, 4.59 wt% and 8.87 wt% in NVPP, NFPP and NMPP, respectively.

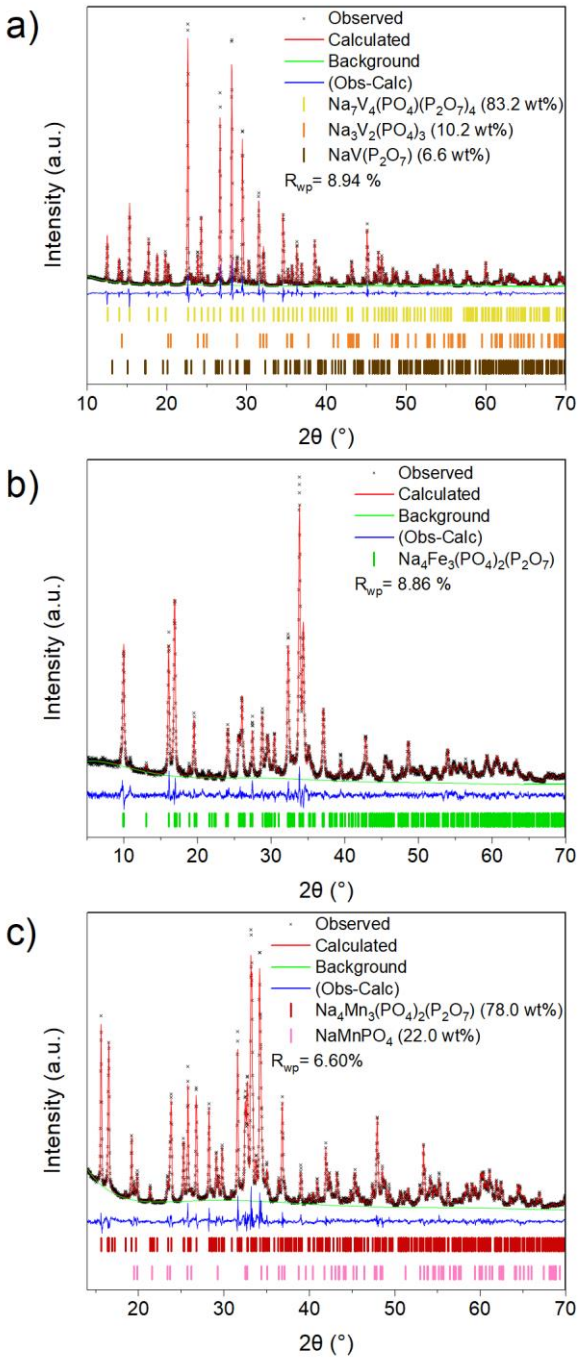

Figure 1. Powder X-ray diffraction patterns of (a) NVPP, (b) NFPP and (c) NMPP. The reference patterns are obtained from the literature.[21,30,32–35]

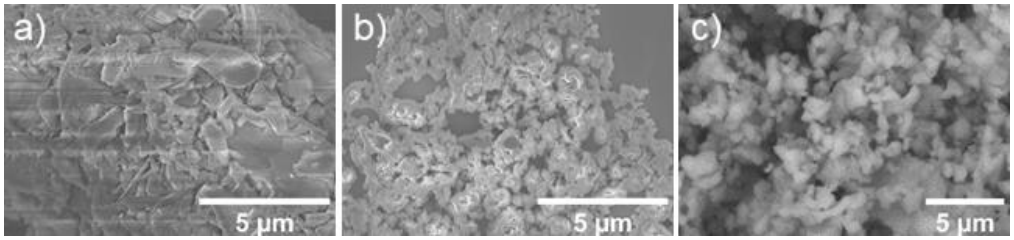

Figure 2. SEM images of (a) NVPP, (b) NFPP and (c) NMPP samples.

Electrochemical Characterization

CV was performed on three representative electrodes in T-type cells for the initial electrochemical characterization using organic 1M $NaPF_6$ in diglyme and aqueous 17m $NaClO_{4(aq.)}$ electrolytes. The voltammograms were recorded at 0.5 mV s^{-1} scan rate and are presented in Figure 3. The NVPP displays several well pronounced and reversible current peaks in both electrolytes (Figure 3 (a)). The first set of small reversible peaks at 3.40/3.35 V and 3.49/3.45 V vs Na^+/Na for organic and aqueous electrolytes, respectively, are attributed to the $V^{(III)}/V^{(IV)}$ redox transition originating from impurity $Na_3V_2(PO_4)_3$.[37] Only two anodic peaks at 3.97/3.89 V in organic, and at 4.05/3.98 V in aqueous electrolyte could be assigned to the $V^{(III)}/V^{(IV)}$ redox transition in NVPP. This suggests a two-stage Na^+ ion deinsertion process:[28]

$$Na_7V_4^{(III)}(PO_4)(P_2O_7)_4 \leftrightarrows Na_5V_2^{(III)}V_2^{4+}(PO_4)(P_2O_7)_4+2Na^++2e^- \quad (1)$$

$$Na_5V_2^{(III)}V_2^{(IV)}(PO_4)(P_2O_7)_4 \leftrightarrow Na_3V_4^{(IV)}(PO_4)(P_2O_7)_4+2Na^++2e^- \quad (2)$$

However, the reversible insertion of Na^+ ions during reduction appears as a single cathodic peak at 3.82 V and 3.87 V in organic and aqueous electrolyte, respectively. This suggests a single-stage reverse process:

$$Na_3V_4^{(IV)}(PO_4)(P_2O_7)_4+4Na^++4e^- \leftrightarrows Na_7V_4^{(III)}(PO_4)(P_2O_7)_4 \quad (3)$$

The NFPP CV results presented in Figure 3 (b) also show several reversible current peaks in the potential range of 2.52-3.26 V and 2.60-3.37 V for organic and aqueous electrolytes, respectively. However, the aqueous electrolyte cell shows lower currents and broader peaks. The peaks correspond to $Fe^{(III)}/Fe^{(II)}$ redox reactions accompanied by de-/insertion of sodium from three different crystallographic sites:[38]

$$Na_4Fe_3^{(III)}(PO_4)_2(P_2O_7) \leftrightarrows Na_3Fe_2^{(II)}Fe^{(III)}(PO_4)_2(P_2O_7)+Na^++e^- \quad (4)$$

$$Na_3Fe_2^{(II)}Fe^{(III)}(PO_4)_2(P_2O_7) \leftrightarrows Na_2Fe^{(II)}Fe_2^{(III)}(PO_4)_2(P_2O_7)+Na^++e^- \quad (5)$$

$$Na_2Fe^{(II)}Fe_2^{(III)}(PO_4)_2(P_2O_7) \leftrightarrows NaFe_3^{(III)}(PO_4)_2(P_2O_7)+Na^++e^- \quad (6)$$

In fact, although sodium occupies four different crystallographic positions in the crystal structure of NFPP with different coordination, one of them is electrochemically inactive.[18] Uneven amount of oxidation and reduction peaks suggest that sodium ions are inserted/extracted in the potential range through an asymmetrical mode.[39]

The CVs for NMPP recorded in organic and aqueous electrolytes are presented in Figure 3 (c). The voltammograms for the first cycle do not display any prominent current peaks but only broad features in the studied potential range from 2.9 to 4.1 V vs Na^+/Na. These features disappear completely in later CV cycles. As it is discussed later from the galvanostatic cycling data, this might be related to either limited electrochemical activity or very fast capacity loss of NMPP.

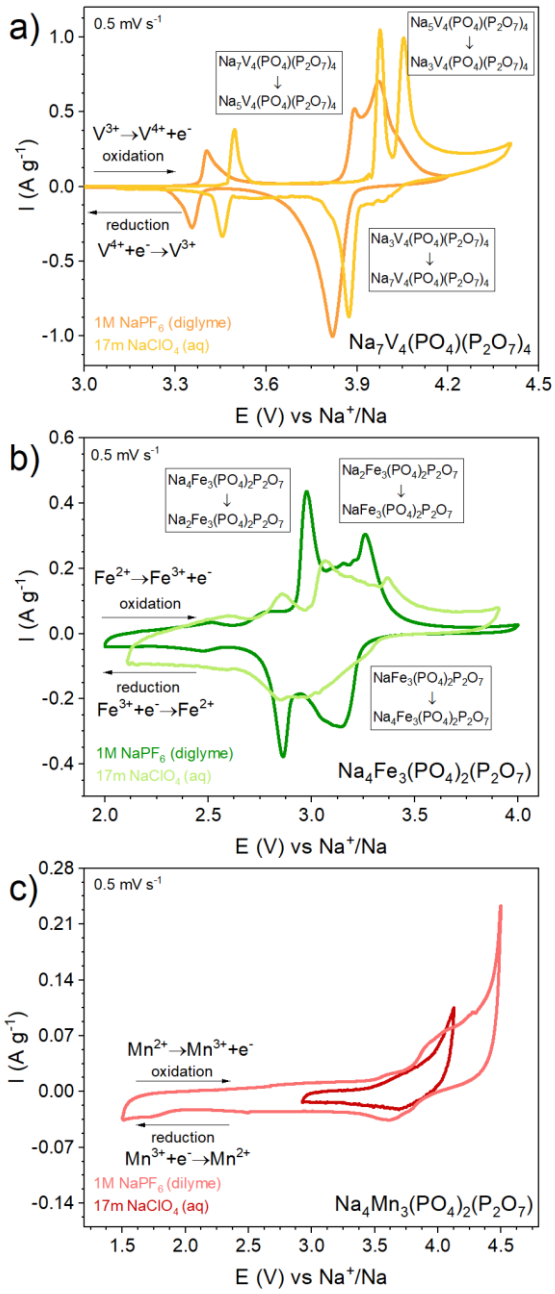

Figure 3. Cyclic voltammograms for the first cycle of (a) NVPP, (b) NFPP, and (c) NMPP electrodes recorded in 1M $NaPF_6$ (diglyme) and 17m $NaClO_{4\ (aq)}$ electrolytes at 0.5 mV s^{-1} scan rate.

The GCD cycling of NVPP was carried in four different electrolytes: organic 1M $NaPF_6$ in diglyme or EC:DEC (3:7, vol%), and aqueous 1M Na_2SO_4 or 17m $NaClO_4$. The GCD rate was calculated with respect to the theoretical specific capacity of NVPP, *i.e.,* 1C = 0.093 A g^{-1}. One hundred GCD cycles were performed in the potential range of 2.5 - 4.2 V vs Na^+/Na. The results in organic electrolytes presented in Figure 4 (a) show similar performance in both cases. The galvanostatic potential profiles of NVPP exhibit two close plateaus at 3.88 and 3.98 V vs Na^+/Na during charging and a single plateau at 3.86 V during discharging. Additional small

plateaus at 3.41 and 3.36 V vs Na^+/Na correspond to NVP impurity. These features agree well with CV results. The initial capacity and its retention after 100 cycles at 1C are 78.7 mAh g^{-1} and 82.7%, and 79.7 mAh g^{-1} and 84.6% for diglyme and EC:DEC electrolytes, respectively. These results suggest NVPP as a very stable material with good electrochemical performance. The same tests were performed in aqueous electrolytes in the potential range 0.2 - 1.15 V vs Ag/AgCl (3.13 - 4.08 V vs Na^+/Na). The results presented in Figure 4 (b) indicate a significantly poorer performance of NVPP in aqueous electrolytes. The NVP plateau (from impurities) disappears faster than those of NVPP, suggesting that the NVPP framework is slightly more stable in an aqueous environment than that of NVP. The initial capacity and its retention after 100 cycles at 1C are 54.8 mAh g^{-1} and 2.4%, and 51.4 mAh g^{-1} and 18.7% for 1M Na_2SO_4 and 17m $NaClO_4$ electrolytes, respectively. The results suggest very rapid degradation of NVPP in low concentration aqueous electrolyte, which is not significantly improved even by the use of high concentration 'water-in-salt' electrolyte. This is most likely related to the dissolution and stability of $V^{(V)}$ species in aqueous environments, as it is also indicated by the lower Coulombic efficiency observed in aqueous systems. The detailed mechanism of V-based polyanionic phosphate degradation in aqueous solutions will be addressed in our upcoming *in situ/operando* study.

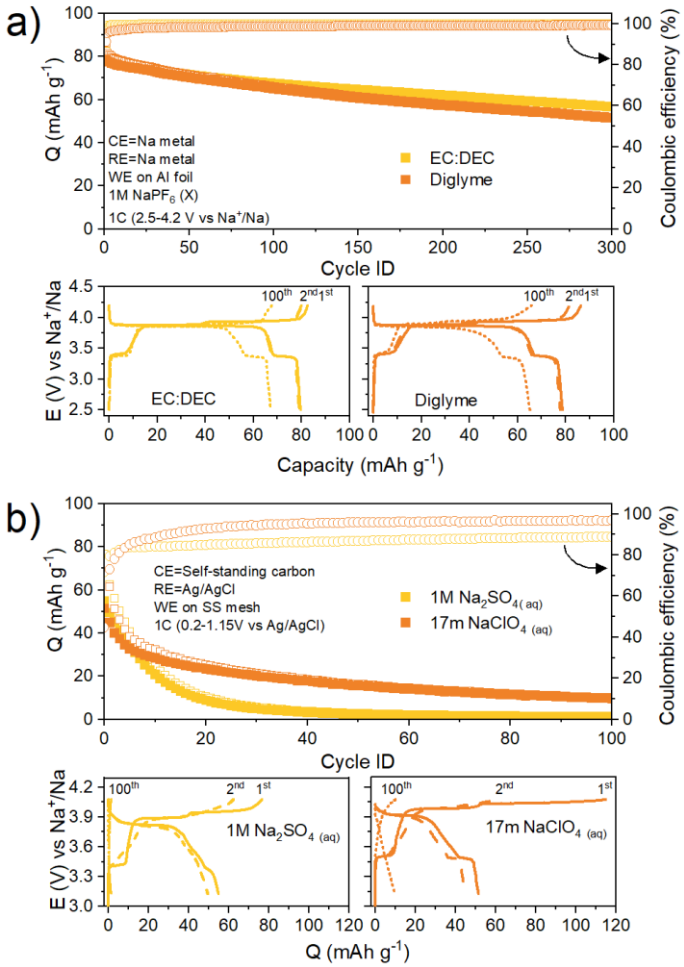

Figure 4. Galvanostatic charge-discharge cycling performance of NVPP in (a) organic and b) aqueous electrolytes at 1C rate.

The rate capability of NVPP was evaluated in organic diglyme-based electrolyte only due to low cycling stability in all studied aqueous electrolytes. A set of different specific currents corresponding to 0.1, 0.2, 0.5, 1, 2, 5, 10 and 20C were used to evaluate the rate capability. The results are summarized in Figure 5. The specific capacity at 0.1C rate was 81.5 mAh g^{-1}, decreased to 60.4 mAh g^{-1} when switched to 1C, and was negligible at 20C. However, the capacity was recovered when the rate was switched back to 0.1C. The plateaus in potential profiles shift to higher potentials at higher currents and become virtually indistinguishable at very high rates indicating significant polarization effects. The results show a decent and well recoverable rate performance of NVPP in organic-based electrolytes.

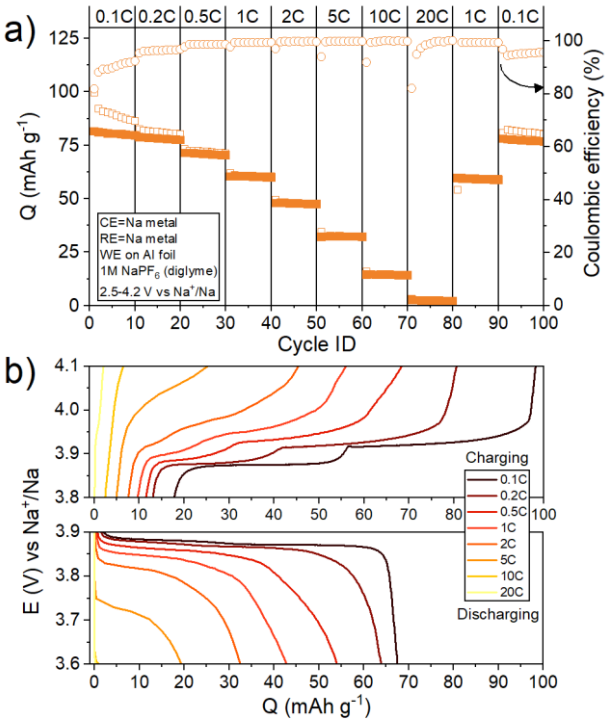

Figure 5. Galvanostatic rate capability of NVPP in organic diglyme electrolyte. a) specific capacity vs cycle number and b) capacity vs. potential.

The GCD cycling of NFPP was also performed in both organic- and aqueous-based electrolytes. The 1C rate equal to 0.129 A g^{-1} was estimated based on the theoretical capacity of NFPP, and the selected potential range was 1.8 - 4.0 V vs Na^+/Na and -0.4 - 0.8 V vs Ag/AgCl (2.53 - 3.73 V vs Na^+/Na) for organic and aqueous systems, respectively. The electrochemical performance in organic-based electrolytes is presented in Figure 6 (a). The initial capacity and its retention after 100 GCD cycles are 86.0 mAh g^{-1} and 94.9%, and 89.9 mAh g^{-1} and 69.4% in diglyme and EC:DEC electrolytes, respectively. The better performance of the diglyme-based with respect to traditional EC:DEC electrolyte could be attributed to the different chemical composition, narrower distribution, thickness, and stability of the solid electrolyte interphase (SEI) and the cathode electrolyte interphase (CEI) on the Na and the positive (cathode) electrode formed in diglyme electrolyte.[40,41]

Four different aqueous electrolytes, namely, 1M Na_2SO_4, 17m $NaClO_4$, 8m NaTFSI, and

28m Kac + 8m NaAc were tested using NFPP as cathode (Figure 6 (b)). The initial specific capacity and its retention after 100 cycles are 60.1 mAh g^{-1} and 43.9% in 1M $Na_2SO_{4\ (aq.)}$, 53.5 mAh g^{-1} and 59.4% in 17m $NaClO_{4\ (aq.)}$, 54.5 mAh g^{-1} and 11.2% in 8m $NaTFSI_{(aq.)}$, and 33.4 mAh g^{-1} and 27.2% for 28m Kac + 8m $NaAc_{\ (aq.)}$. The initial capacity and its retention in aqueous electrolytes are significantly lower than in organic systems. Only a slightly better performance is shown by NFPP in 1M $Na_2SO_{4\ (aq.)}$ and 17m $NaClO_{4\ (aq.)}$, whereas 'water-in-salt' electrolytes are even worse. Interestingly, the potential profiles at 1C show significantly more sloping in aqueous electrolytes, which could imply some kinetic limitations. These, as discussed later, might be due to some resistive interphasial layer formation from electrode or electrolyte degradation products.

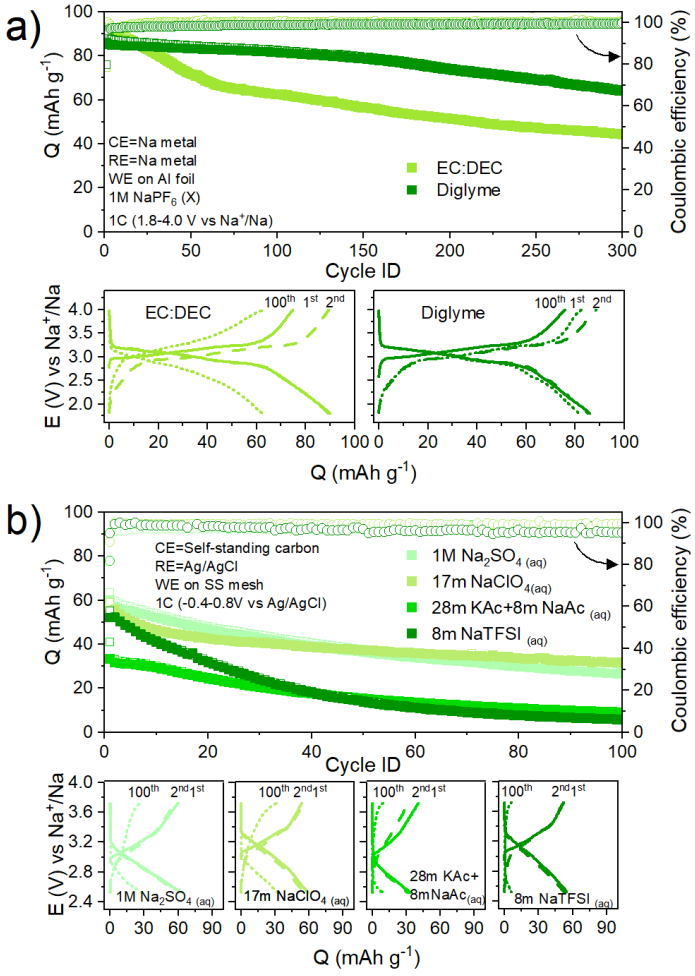

Figure 6. Galvanostatic charge-discharge cycling performance of NFPP in different (a) organic and (b) aqueous electrolytes at 1C rate.

The rate capability of NFPP was evaluated in organic diglyme based and aqueous 17m $NaClO_4$ electrolytes due to the previously observed electrochemical performance. A set of different specific currents corresponding to 0.1, 0.2, 0.5, 1, 2, 5, 10 and 20C were used to evaluate the rate capability. The results are summarized in Figure 7. In the case of organic electrolyte, the specific capacity at 0.1C rate is 93.9 mAh g^{-1}, decreases only to 49.1 mAh g^{-1}

at 20C and is fully recovered to 93.3 mAh g^{-1} after the rate was switched back to 0.1C. This indicates an excellent rate capability of NFPP in organic electrolytes. On the other hand, the specific capacity was only 29.3 mAh g^{-1} at 0.1C rate and dropped to negligible values at 20C, although coming back to 13.8 mAh g^{-1} at 0.1C again in aqueous systems. The poor rate capability certainly points to some kinetic limitations of NFPP in aqueous electrolytes. Another interesting observation is that the charge capacity at 0.1C was even lower than at 1C rate. This obviously indicates some dissolution-based degradation mechanisms because the longer time the electrode spends in the electrolyte results in lower capacities. Whether this is related to Fe dissolution or instability of the mixed phosphate-pyrophosphate framework requires additional studies.[17] Knowing the mechanism would allow the design of some degradation mitigation strategies based on protective coatings or electrolyte additives. One hypothesis to explain this could be based on the importance of pH in aqueous electrolytes. Higher pH values expected in such electrolytes as 28m KAc+8m NaAc $_{(aq.)}$ not only result in higher aqueous stability of FeO_4^{-2} (according to the Pourbaix diagram), but also significantly stronger instability of phosphates.[42] Near neutral or even slightly acidic pH (due to dissolved CO_2) of aqueous Na_2SO_4 and $NaClO_4$ could result in better NFPP framework stability and better capacity retention. Overall, NFPP seems to be an excellent electrode material for organic Na-ion batteries and could likely be enabled in aqueous systems by understanding of its degradation mechanism and designing an appropriate prevention strategy.

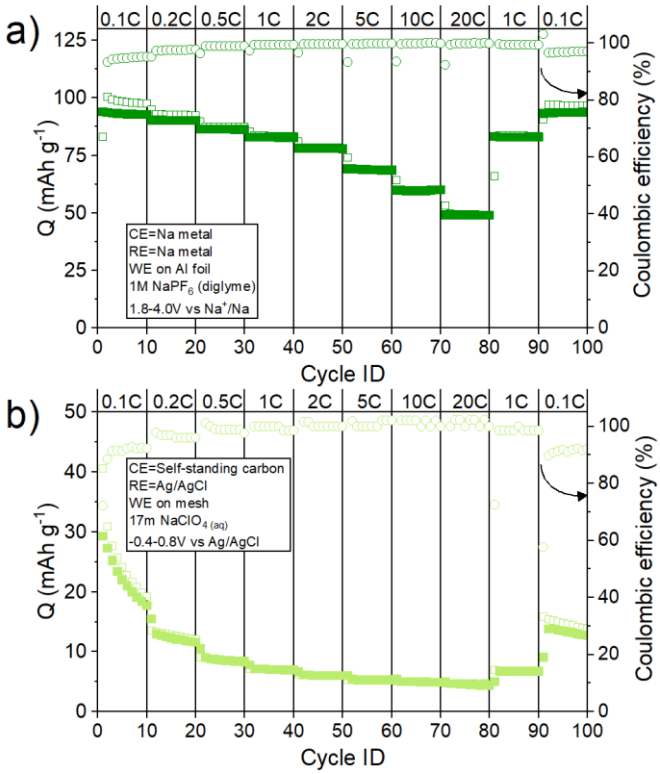

Figure 7. Galvanostatic rate capability of NFPP at different C-rates in (a) 1M $NaPF_6$ (diglyme) and (b) 17m $NaClO_{4(aq)}$ electrolytes.

The GCD cycling of NMPP was also performed in 1M $NaPF_6$ (EC:DEC) and 17m $NaClO_4$ $_{(aq.)}$ electrolyte solutions. The 1C rate equal to 0.129 A g^{-1} was estimated based on the theoretical

capacity of NMPP, and the chosen potential range was 1.7 - 4.5 V vs Na^+/Na and 0 - 1.2 V vs Ag/AgCl (2.93 - 4.13 V vs Na^+/Na) for organic and aqueous systems, respectively (Figure 8). The initial capacity and its retention after 100 cycles at 1C are 19.9 mAh g^{-1} and 50.1%, and 7.8 mAh g^{-1} and 75.0% in organic and aqueous electrolytes, respectively. Our previous results in low concentration 1M $Na_2SO_{4\ (aq.)}$ electrolytes also showed very fast degradation.[25] In contrast to previous reports of a successful operation of NMPP,[21,26] the present results show only very limited electrochemical activity also in organic electrolytes and virtually no activity in 'water-in-salt' electrolytes. As discussed in our previous study,[25] there is certainly significant Mn dissolution into the electrolyte due to the stability of $Mn^{(II)}_{(aq.)}$ species, but this could not explain the entire capacity loss as most of the Mn still stays in the electrode after cycling. The result of this study in organic and high concentration aqueous electrolytes also suggest that there must be some other mechanisms which make NMPP and likely similar $Mn^{(II)}$-based framework materials electrochemically inactive. This could result from the formation of insoluble and inactive phases, which form blocking layers on electrode particles during the initial cycles, limiting the performance of these materials as potential battery electrodes.

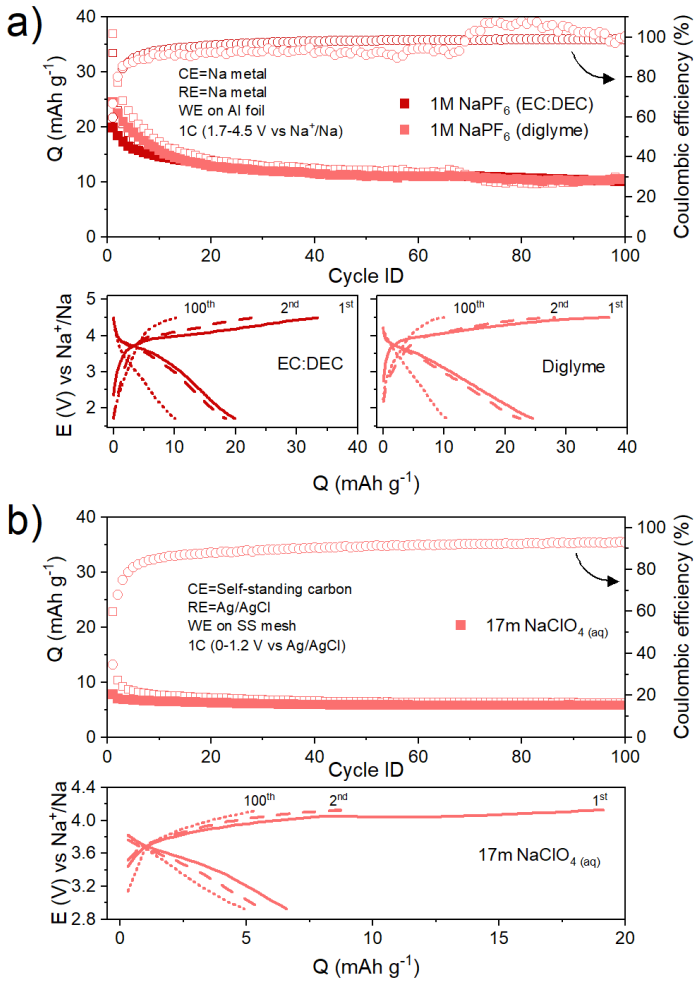

Figure 8. Galvanostatic cycling performance of NMPP electrodes in (a) 1M $NaPF_6$ (diglyme) and (b) 17m $NaClO_{4(aq)}$ electrolytes at 1C rate.

CONCLUSIONS

In this work three different V-, Fe-, and Mn-based mixed polyanionic phosphate-pyrophosphate compounds: $Na_7V_4(PO_4)(P_2O_7)_4$, $Na_4Fe_3(PO_4)_2P_2O_7$, and $Na_4Mn_3(PO_4)_2P_2O_7$ were successfully prepared by solid-state synthesis methods. The electrochemical properties of these materials as Na-ion battery electrodes are comprehensively characterized in different organic, high, and low concentration aqueous electrolytes.

- The results show $Na_7V_4(PO_4)(P_2O_7)_4$ as suitable electrode material with good cycling performance and rate capability in organic solvent-based electrolytes. However, it performs poorly in aqueous and even in 'water-in-salt' electrolytes. The rapid electrochemical degradation is most likely related to the dissolution and aqueous stability of $V^{(V)}$ species in aqueous environments. These results suggest that V might not be the most optimal transition metal in mixed phosphate-pyrophosphate systems for aqueous-based systems, and additional stabilization strategies need to be employed.
- The results for $Na_4Fe_3(PO_4)_2P_2O_7$ show it to be a well performing electrode material for organic Na-ion batteries with good cycling stability and rate capability. The results in aqueous systems indicate some degradation mechanism related to Fe dissolution or instability of the mixed phosphate-pyrophosphate framework, which results in kinetic limitations of this material. Further understanding of this mechanism might allow the design of a mitigation strategy either based on protective coatings or electrolyte additives, which could enable this material for aqueous applications.
- In agreement with several other previous reports, $Na_4Mn_3(PO_4)_2P_2O_7$ is shown to have only very limited electrochemical activity in organic electrolytes and virtually no activity in 'water-in-salt' electrolytes. The results suggest that some degradation processes occur, similar to other $Mn^{(II)}$-based framework materials, making them electrochemically inactive and unstable. This could be a result of the formation of insoluble/inactive phases resulting in blocking layers on electrode particles during the initial cycles, limiting the performance of this and similar materials.

Acknowledgements

G.G. acknowledges the fellowship from the Deutsche Bundesstiftung Umwelt (DBU). G.G., J.P. and L.V. acknowledge funding from the European Regional Development Fund (Project No. 01.2.2-LMT-K-718–02–0005) under a grant agreement with the Research Council of Lithuania (LMTLT). G.G., M.Z. and S.P. acknowledge the basic funding from the Helmholtz Gemeinschaft.

REFERENCES

[1] B. Dunn, H. Kamath, J.-M. Tarascon, *Science* **2011**, 334, 928–935.
[2] H. Zhang, I. Hasa, S. Passerini, *Adv. Energy Mater.* **2018**, 8, 1702582.
[3] C. Vaalma, D. Buchholz, M. Weil, S. Passerini, *Nat. Rev. Mater.* **2018**, 3, 1–11.
[4] C. Delmas, *Adv. Energy Mater*. **2018**, 8, 1703137.
[5] Y. Fang, J. Zhang, L. Xiao, X. Ai, Y. Cao, H. Yang, *Adv. Sci.* **2017**, 4, 1600392.

[6] C. Masquelier, L. Croguennec, *Chem. Rev.* **2013**, 113, 6552–6591.
[7] B. Senthilkumar, C. Murugesan, L. Sharma, S. Lochab, P. Barpanda, *Small Methods* **2019**, 3, 1800253.
[8] L. He, H. Li, X. Ge, S. Li, X. Wang, S. Wang, L. Zhang, Z. Zhang, *Adv. Mater. Interfaces* **2022**, 9, 2200515.
[9] W. Yang, Q. Liu, Y. Zhao, D. Mu, G. Tan, H. Gao, L. Li, R. Chen, F. Wu, *Small Methods* **2022**, 6, e2200555.
[10] T. Jin, H. Li, K. Zhu, P.-F. Wang, P. Liu, L. Jiao, *Chem. Soc. Rev.* **2020**, 49, 2342–2377.
[11] Y. Yuan, Q. Wei, S. Yang, X. Zhang, M. Jia, J. Yuan, *Energy Storage* **2022**, 50, 760-782.
[12] Y. Niu, Y. Zhang, M. Xu, *J. Mater. Chem. A* **2019**, 7, 15006-15025.
[13] A. Zhao, Y. Fang, X. Ai, H. Yang, Y. Cao, *J. Mater. Chem.* **2021**, 60, 635-648.
[14] H. Kim, I. Park, S. Lee, H. Kim, K.-Y. Park, Y.-U. Park, H. Kim, J. Kim, H.-D. Lim, W.-S. Yoon, K. Kang, *Chem. Mater.* **2013**, 25, 3614–3622.
[15] F. Sanz, C. Parada, J. M. Rojo, C. Ruíz-Valero, *Chem. Mater.* **2001**, 13, 1334–1340.
[16] H. Kim, I. Park, D.-H. Seo, S. Lee, S.-W. Kim, W. J. Kwon, Y.-U. Park, C. S. Kim, S. Jeon, K. Kang, *J. Am. Chem. Soc.* **2012**, 134, 10369–10372.
[17] A. J. Fernández-Ropero, M. Zarrabeitia, M. Reynaud, T. Rojo, M. Casas-Cabanas, *J. Phys. Chem. C* **2018**, 122, 133–142.
[18] X. Pu, H. Wang, T. Yuan, S. Cao, S. Liu, L. Xu, H. Yang, X. Ai, Z. Chen, Y. Cao, *Energy Storage Mater.* **2019**, 22, 330–336.
[19] M. H. Lee, S. J. Kim, D. Chang, J. Kim, S. Moon, K. Oh, *Mater. Today* **2019**, 29, 26-36.
[20] J. Gao, Y. Mei, L. Ni, H. Wang, B. Song, W. Deng, G. Zou, H. Hou, X. Ji, *Inorg. Chem.* **2023**, 62, 23, 9099–9110.
[21] H. Kim, G. Yoon, I. Park, K.-Y. Park, B. Lee, J. Kim, Y.-U. Park, S.-K. Jung, H.-D. Lim, D. Ahn, S. Lee, K. Kang, *Energy Environ. Sci.* **2015**, 8, 3325–3335.
[22] H. Xu, J. Ma, X. He, J. Sun, L. Yang, R. Jiang, Z. Lei, Z.-H. Liu, Q. Li, *Nanoscale* **2023**, 15, 4830–4838.
[23] H. Kim, G. Yoon, I. Park, J. Hong, K.-Y. Park, J. Kim, K.-S. Lee, N.-E. Sung, S. Lee, K. Kang, *Chem. Mater.* **2016**, 28, 7241–7249.
[24] A. Gezović, M. J. Vujković, M. Milović, V. Grudić, R. Dominko, S. Mentus, *Energy Storage Mater.* **2021**, 37, 243–273.
[25] D. Tediashvili, G. Gečė, J. Pilipavičius, S. Daugėla, T. Šalkus, J. Juodkazytė, L. Vilčiauskas, *Electrochim. Acta* **2022**, 417, 140294.
[26] S. Ryu, J. E. Wang, J.-H. Kim, R. Ruffo, Y. H. Jung, D. K. Kim, *J. Power Sources* **2019**, 444, 227274.
[27] S. Y. Lim, H. Kim, J. Chung, J. H. Lee, B. G. Kim, J.-J. Choi, K. Y. Chung, W. Cho, S.-J. Kim, W. A. Goddard 3rd, Y. Jung, J. W. Choi, *Proc. Natl. Acad. Sci.* **2014**, 111, 599–604.
[28] C. Deng, S. Zhang, *ACS Appl. Mater. Interfaces* **2014**, 6, 9111–9117.
[29] B. H. Toby, R. B. Von Dreele, *J. Appl. Cryst.* **2013**, 46, 544-549.
[30] L.-M. Zhang, N.-Q. Ren, S. Wang, W.-J. Deng, F. Chen, Z.-Y. Wen, C.-H. Chen, *ACS Appl. Energy Mater.* **2021**, 4, 10298–10305.
[31] W. Fang, Z. An, J. Xu, H. Zhao, J. Zhang, *RSC Adv.* **2018**, 8, 21224–21228.
[32] M. Chen, W. Hua, J. Xiao, D. Cortie, W. Chen, E. Wang, Z. Hu, Q. Gu, X. Wang, S. Indris, S.-L. Chou, S.-X. Dou, *Nat. Commun.* **2019**, 10, 1480.

[33] Y. P. Wang, K. H. Lii, S. L. Wang, *Acta Crystallogr. C* **1989**, 45, 1417–1418.
[34] I. V. Zatovsky, *Acta Crystallogr. Sect. E Struct. Rep. Online* **2010**, 66, i12.
[35] J. Moring, E. Kostiner, *J. Solid State Chem.* **1986**, 61, 379–383.
[36] G. Plečkaitytė, M. Petrulevičienė, L. Staišiūnas, D. Tediashvili, J. Pilipavičius, J. Juodkazytė, L. Vilčiauskas, *J. Mater. Chem. A* **2021**, 9, 12670–12683.
[37] H. Zhang, B. Qin, D. Buchholz, S. Passerini, *ACS Appl. Energy Mater.* **2018**, 1, 6425–6432.
[38] X. Ma, Z. Pan, X. Wu, P. K. Shen, *Chem. Eng. J.* **2019**, 365, 132–141.
[39] X. Ma, X. Wu, P. Shen, *ACS Appl. Energy Mater.* **2018**, 1, 6268–6278.
[40] K. Westman, R. Dugas, P. Jankowski, *ACS Appl. Energy* Mater. **2018**, 1, 6, 2671-2680.
[41] B. Qin, M. Zarrabeitia, A. Hoefling, Z. Jusys, X. Liu, J. Tübke, R. J. Behm, G. Cui, A. Varzi, S. Passerini, *J. Power Sources* **2023**, 560, 232630.
[42] V. Radtke, D. Stoica, I. Leito, F. Camões, I. Krossing, B. Anes, M. Roziková, L. Deleebeeck, S. Veltzé, T. Näykki, F. Bastkowski, A. Heering, N. Dániel, R. Quendera, L. Liv, E. Uysal, N. Lawrence, *Pure Appl. Chem.* **2021**, 93, 1049–1060.